PARAMETRIC EVALUATION OF A CENTRIFUGAL PUMP USING ANSYS SOFTWARE

B. Sibambo [1], T. Jamiru [1] and T.A. Adegbola [1]

Faculty of Engineering and Built Environment
Department of Mechanical and Mechatronics Engineering,
Tshwane University of Technology, Gauteng, Pretoria, 0183, South Africa,

Corresponding Authors Email: sibambob@tut.ac.za

Article History: Received 22 February 2025; Revised 26 November 2025; Accepted 29 December 2025

ABSTRACT: The centrifugal pump's performance is affected by different parameters and the flow inside the pump is complicated. The ANSYS computational fluid dynamics technique is an excellent tool to solve complex flows inside the pump and aid engineers in designing and predicting the pump's optimal performance for specific applications. The objective of the study is to conduct parametric evaluation with a specific focus to determining the effect of the various impeller blade numbers on the performance curve of the centrifugal pump. The iterations made were the impeller blade numbers and the volumetric flow rates. The rotational speed of 1450 rpm was utilised and the head rise of 20 m. Outcome: An increase in blade numbers translates to an increase in head and pressure of the system. Furthermore, it was discovered that when the blade numbers are increased, the power consumption of the pump also increases. The best efficiency points were observed for the 4, 6 and 8-blade configurations at the volumetric flow rate of 396 m^3/hr while the 10-blade configuration best efficiency was at 324 m^3/hr. Beyond the best efficiency points the efficiency for the 4 and 6-blades dropped marginally while the 8 and 10-blades dropped steeply.

KEYWORDS: *Impeller, Head, Efficiency, Power, Volumetric Flow Rate*

1.0 INTRODUCTION

The industrial, agricultural and domestic sectors utilize centrifugal pumps extensively for various purposes such as irrigation, distribution, dewatering, slurry, sewage etc. The main purpose of the pump is to transport fluid media from a region of low-pressure region to a high-pressure region, it is also cheaper to conduct maintenance due to less wear and tear. At the inlet of the pump fluid pressure rises and continuously do so radially outward the impeller blades until it reaches the volute casing outlet, this rise in pressure is facilitated by the conversion of mechanical energy to pressure energy from the pump motor through the shaft which turns the centrifugal pump impeller. There are various types of impellers namely open, semi-open and closed. The closed impeller has 2 disks closing vanes on both sides while semi-open type has only 1 disk closing on one side and free on the other, lastly the open type which has no disks enclosing the vanes.

"The overall efficiency is high for rotodynamic pumps. Hence these are the most popular pumps in use. Rotodynamic pumps can be of radial flow, mixed flow and axial flow types according to the flow direction. Centrifugal pumps generally handle lower volumes at higher pressures. Mixed flow pumps handle comparatively larger volumes at medium

range of pressures. Axial flow pumps can handle very large volumes, but the pressure against which these pumps operate is limited. The overall efficiency of the three types is nearly the same" [1].

Rosa and Emerick [2] stated that the fluid flow media can be analyzed utilizing the optimum tool termed computational fluid dynamics (CFD). The pump engineer has the ability to generate optimal results with the aid of CFD tool, this is due to accurate prediction of fluid flow patterns inside the centrifugal pump during various operating conditions.

The focus area of this research paper is to investigate the effect of various number of impeller blades and volumetric flow rate on pump head, efficiency and power consumption under steady state working conditions. The ANSYS CFD software will also be utilized for the simulation and appropriate selection of the optimal impeller geometry of the overall performance of the centrifugal pump.

1.1 LITERATURE REVIEW

Lopez et al. [3] carried out the study to design and evaluate output pressure and velocity contours of the centrifugal pump impeller performance when the specific velocity of 0.27 was applied. The authors discovered that as the velocity enters the impeller it has a lower value, however as soon as it reaches the blades it yields higher values. Similar situation can be described about the pressure at the inlet which is the suction area, it continues to increase as it approaches exit blade section of the pump impeller. The pressure head is identified when the volumetric flow rate is at zero and continues to gradually decrease with an increment in flow rate.

Rajmane and Kallurkar [4] conducted a study to analyze the stresses and displacements developed on the centrifugal pump impeller when the impeller is rotated at various speeds. Authors conducted first principle calculations to design an impeller in accordance with specifications of the customer, the dimensions were utilized to create a computer aided design model (Impeller and casing constructed of mild steel) utilizing CATIA software.

It was discovered that all stresses developed for varying rotational speed iterations in FEA were all within allowable limits, however the increment in rotational speed yield a higher value of stress. Furthermore, the displacements also increase with an increase in rotational speed. Concluding remarks of authors were that all stresses and displacements generated under various iterations in rotational speed were all within allowable limits and hence the designs were safe for operational purposes.

Muttalli et al. [5] undertook a research study to evaluate the centrifugal pump's efficiency, pressure head, power and cavitation when various iterations of rotational speeds 7000, 7700, 8400 and 9100 rpm as well as mass flow rates from 0 to 220 liters per minute (L/min) were applied. Findings for the pressure head of the pump was that a low rotational speed will yield less head in comparison with the pump adjusted to a higher rotational speed of the impeller. Moreover, as the mass flow rate of the pump fluid increase, the pressure

head is gradually decreased when the rotational speed remains constant, this can be attributed to the losses generated as mass flow rate is increasing. As the rotational speed remains constant with respect to power evaluation, it is discovered that an increment in mass flow rate is directly proportional to the input power from the motor. Finally, the rotational speed of the impeller and increment in mass flow rate facilitates the formation of cavitation.

Marathe and Saxena [6] investigated the effect of exit blade angles that facilitates development of cavitation phenomenon during operating condition of a centrifugal pump when the flow rate is reiterated. Authors discovered that the water vapours inside the pump casing increase when a lower exit blade angle is applied and gradually increased to the higher one. Furthermore, the difference in density between liquid water and vapour is evident on the CFD model, the water is settling at the bottom of the pump casing while water vapour is identified at the top portion of the casing. The pressure contours on the CFD models depicts a decline trend as the mass flow rate is increased from 1.5 L/s to 5 L/s. The Net Positive Suction Head required increase with an increase in mass flow rate and this will lead to cavitation when Net Positive Suction Head (NPSH) value is extremely high.

Furthermore, they recommend the utilization of exit blade angle around a range of 200 to 300 as they have less chance to develop cavitation in comparison to higher exit blade angles, and are more efficient and provide high pump performance.

High vibrations in pumps are the result of cavitation as well as misalignment of couplings between the pump and motor in some instances. The damage to impeller leads to drop in pump efficiency while power consumption rises. “Flow separation is due to the pressure difference between the trailing and leading edge”, this is due to the speed and the shape of the impeller. Commonly, the pump efficiency will decrease significantly during flow separation and back flow of fluid continue to decrease as damage to the impeller increases” [1].

Hayder [7] conducted a study to discover the effect of applying number of impeller blades from 5 to 16 have on centrifugal pump’s performance, the three cases were investigated while all other parameters remain constant. Upon conducting CFD for the first case, it was discovered that the highest pressure was recorded when the number of blades were 10 and the lowest pressure when the number of blades was 8 when the pressure head of 25m and rotational speed of 3500 rpm were applied. The second case, the number of blades to yield high pressure was 9 while the lowest pressure was achieved by 16 blades for the rotational speed of 3800 rpm and pressure head of 28 m. The highest pressure was obtained by 8 blades and lowest pressure by 6 blades for the third case when the rotational speed of 4000 rpm and pressure head of 30 were applied. Concluding remarks of the author was that the appropriate number of blades can be selected based on the requirements of the client for optimum operational efficiency of the pump.

Eliyamin et al. [8] investigated the influence of adding impeller blades on a centrifugal pump device using ANSYS Fluent module at the constant rotational speed of 2800rpm. The impeller blades of interest were 5, 7 and 9 respectively, prior to conducting a

ISSN 2180-1053 e-ISSN 2289-8123 Vol.17 No.2

numerical study, an experiment was conducted on a pump under identical operating parameters with the exception of 5 and 9-bladed impellers. The authors discovered that the experimental results were in well agreement with the numerical investigation for the 7-blade impeller configuration. In addition, it was uncovered that the highest efficiency and head were achieved through the 7-blade impeller configuration, owing to the rationale that increasing the blade numbers to a certain point results in closing the pitch ratio between the blades which leads to less distorted velocity flow fields and that translate into minimal secondary flow losses.

Authors also indicated that for the case of 5-blade impeller, they observed the secondary flow and jet/wake were predominant at the impeller blade exit region, this is due to large pitch ratio which cause non-uniform fluid flows and high losses. It was also discovered that the secondary flow and mixing losses were less dominant for the case of 9-blade impeller. The reduction of pitch ratio between blades resulted in narrower flow channels which led to increased friction losses overall. In conclusion, authors indicated that the optimal impeller configuration was the 7-blade impeller, in second position was the 5-blade impeller and not so optimal was the 9-blade impeller.

Enemugha et al. [9] Carried out a numerical study using ANSYS Fluent to determine the influence of increasing number of blades on a centrifugal pump and using polynomial regression models. The blades number of interest ranged from 4 to 7 with a volumetric flow rate ranging from 100 to 400m^3/h and the variable rotational speed from 1500 to 4500rpm with the aim to discover the optimal balance of hydraulic head and efficiency. The authors observed that the 5-blade impeller achieved the optimum balance by recording the hydraulic efficiency of 91.9% and head of 28.1m compared to other impeller blade configurations.

Moreover, fluid dynamics were improved by increasing the number of blades which resulted in enhanced pressure and velocity distribution, minimizing the fluctuations of pressure in the system. The higher the number of blades, the more hydraulic frictional losses and turbulences were observed. A compromise between hydraulic head and efficiency were observed when the 7-blade impeller achieved a head of 64.1 m at the expense of a reduction in efficiency of 79.5 % when the rotational speed of 4500 rpm was applied.

Venkatratnam [10] has investigated the operational performance of the centrifugal pump considering pressure head and efficiency by the application of iterations in number of blades, rotational speed and volumetric flow rate. The author discovered that as the flow rate is increasing, there is a gradual decrease in pressure head and in contrast the vicinity with low flow rate yield high pressure. Furthermore, the high pressure was identified near the hub and low pressure near the shroud area. The results obtained from CFD analysis for efficiency closely match those conducted from 1st principle calculation and this means boundary conditions applied for CFD analysis were done properly and CFD is the best analysis tool to perform solution approximations to match real life scenarios. Moreover, it was discovered when the 7-bladed impeller was applied at a flow rate of 32kg/s for the rotational speed of 2000rpm, the iteration yielded the best pump efficiency in comparison with others, also the optimum pressure head was achieved when the flow

rate of 22kg/s and a rotational speed of 4000rpm was applied and the number of blades was 6.

1.2 COMPUTATIONAL FLUID DYNAMICS

The most economical strategy prior to pump design and fabrication is to conduct the pump performance prediction. The in-depth knowledge of the complex fluid flow patterns inside the various components of the pump becomes of paramount importance [11]. The most reliable and accurate method to predict pump performance is to conduct a physical experiment, however this approach is tiring, consumes a lot of time and is not economical. [11]stated an alternative approach to compute pump performance prediction is to conduct theoretical calculations. However, this approach has a demerit in the sense that it does not explicitly determine the root cause of unsatisfactorily performance.

The rapid prediction of complicated flow patterns inside the centrifugal pump is made possible through the utilisation of CFD tool. [12] stated that recently CFD has gained reputation pertaining to the inbuilt advanced algorithms to solve complex flow patterns and excellently predict the performance in turbomachines. In general, the CFD is the most preferred tool of choice to solve extremely difficult fluid flow patterns in the turbomachinery industry [13].

2.0 METHODOLOGY

2.1 Design Specification

In a centrifugal pump, performance is governed by several interrelated geometric and hydraulic parameters, table 1 provides parameters of importance considered for the CFD. Head rise reflects the energy imparted to the fluid and determines the pump's ability to overcome system losses, while impeller diameter and rotational speed largely dictate the velocity and therefore the head generated by the impeller. The volumetric flow rate depends on both the impeller design and overall system resistance, and the water density influences the hydraulic power and torque required to drive the pump. Flow quality at the impeller eye is shaped by the inlet flow angle and inlet blade angle, which work together to reduce incidence losses and maintain uniform entry conditions. At the outlet, the exit blade angle sets the tangential velocity component that generates head and contributes to radial thrust. Finally, the number of blades affects flow smoothness, pressure distribution, and efficiency, with designers balancing hydraulic performance against mechanical loading.

Table 1. Pump Duty Parameters

Head Rise (m)	20
Impeller Diameter (m)	0.28
Rotational Speed (RPM)	1450
Volumetric Flow Rate (m^3/hr)	280 to 612
Water Density (kg/m^3)	1000
Inlet Flow Angle (^{0})	90
Inlet Blade Angle (^{0})	25

ISSN 2180-1053 e-ISSN 2289-8123 Vol.17 No.2

Exit Blade Angle (^{0})	33
Number of Blades	4 to 10

2.2 GOVERNING EQUATIONS

2.2.1 Pump Performance

The performance of a centrifugal pump is controlled by the transfer of angular momentum from the rotating impeller to the fluid considered. The core governing relation is the Euler Turbomachinery Equation, which quantifies the theoretical head produced by the pump impeller [14]:

$$H_{\text{th}} = \frac{U_2 W_2 - U_1 W_1}{g} \quad (1)$$

where U is the blade peripheral velocity, and W is the tangential component of absolute velocity at inlet (1) and outlet (2). This equation explicitly explains that the centrifugal pump head is generated by increasing the angular momentum of the fluid. In ideal, inviscid flow, this head would be fully converted to pressure in the volute or diffuser. However, real pumps lose energy to friction, turbulence, and secondary flows. The hydraulic power delivered to the fluid is:

$$P_{hydraulic} = \rho g Q H \quad (2)$$

The overall pump efficiency can be calculated using the following equation

$$\eta = \frac{P_{hydraulic}}{P_{in}} \quad (3)$$

where P_{in} is the shaft input power.

The centrifugal pump performance curves exist due to the viscous flow losses generated inside the pump which are influenced by the variability in the volumetric flow rate. As volumetric flow rate (Q) increases, hydraulic losses rise roughly with the fluid flow, creating the typical decreasing head and volumetric flow rate curve. The Affinity Laws arise through dimensional analysis and similarity theory, express the fundamental scaling of volumetric flow rate (Q) , head (H), impeller diameter (D), and power (P) with shaft rotational speed (N):

$$\frac{Q}{ND^3} = Constant. \quad (4)$$

$$\frac{H}{N^2 D^2} = Constant \quad (5)$$

$$\frac{P}{N^3 D^5} = Constant \quad (6)$$

The specific speed N_S can be determined using equation (7)

ISSN 2180-1053 e-ISSN 2289-8123 Vol.17 No.2

$$N_S = \frac{NQ^{0.5}}{H^{0.75}} \tag{7}$$

The dimensionless number n_S can be computed using equation (8)

$$n_S = \frac{\omega Q^{0.5}}{(gH)^{0.75}} \tag{8}$$

where ω is the angular velocity of the impeller [14].

These relationships work only if dynamic similarity is maintained. This means both Reynolds number and geometric similarity must remain constant. In practice, this condition is often violated. Turbulence, tip leakage, and Reynolds-dependent losses affect results. The pump operates at a point where the head curve meets the system resistance curve. Thus, pump performance must be observed in context with the whole hydraulic system. Deviations from ideal performance in centrifugal pumps are primarily caused by internal flow structures, including boundary layers, recirculation zones, tip-clearance vortices, and diffuser separation. These effects increase entropy generation and reduce the actual head (H_{act}) compared to the theoretical head (H_{th}), such that:

$$H_{\text{act}} = H_{\text{th}} - H_{\text{loss}} \tag{9}$$

Cavitation imposes further constraints: the pressure at the impeller eye must remain above the vapor pressure, as defined by Net Positive Suction Head (NPSH) requirements. If the available NPSH (NPSH_A) drops below the required NPSH (NPSH_R), vapor cavities form and collapse, producing destructive pressure spikes that diminish both performance and service life [14]. Contemporary analyses employing computational fluid dynamics, entropy generation, and unsteady simulations indicate that classical equations remain valid as first-principles descriptors. However, actual pump behavior is governed by complex, three-dimensional, turbulent, and frequently unsteady internal flow phenomena.

2.2.2 Navier Stokes Equations

In this research paper, the fluid under consideration is assumed to be pure water for all numerical simulations and it is incompressible. The research also assumes ambient temperature conditions for the fluid, and the effect of heat transfer in the flow field is ignored.

2.2.2.1 Conservation of Mass: Continuity

The continuity equation for a 3-dimensional fluid flow is expressed in equation (10), since the mass-density for the fluid do not change in x, y, z and t, thus the equation takes the form below [15]:

$$\frac{\partial u}{\partial x} + \frac{\partial v}{\partial y} + \frac{\partial w}{\partial z} = 0 \tag{10}$$

ISSN 2180-1053 e-ISSN 2289-8123 Vol.17 No.2

In equation 10, the variables μ, v *and* ω represent the components of velocity in the x, y and z direction respectively.

2.2.2.2 Conservation of Momentum:

$$\rho\left(\frac{\partial u}{\partial t}+u\frac{\partial u}{\partial x}+v\frac{\partial u}{\partial y}+w\frac{\partial u}{\partial z}\right)=-\frac{\partial \rho}{\partial x}+u\left(\frac{\partial \tau_{xx}}{\partial x}+\frac{\partial \tau_{yx}}{\partial y}+\frac{\partial \tau_{zx}}{\partial z}\right)+\rho F_x \quad (11)$$

$$\rho\left(\frac{\partial v}{\partial t}+u\frac{\partial v}{\partial x}+v\frac{\partial v}{\partial y}+w\frac{\partial v}{\partial z}\right)=-\frac{\partial \rho}{\partial y}+v\left(\frac{\partial \tau_{xy}}{\partial x}+\frac{\partial \tau_{yy}}{\partial y}+\frac{\partial \tau_{zy}}{\partial z}\right)+\rho F_y \quad (10)$$

$$\rho\left(\frac{\partial w}{\partial t}+u\frac{\partial w}{\partial x}+v\frac{\partial w}{\partial y}+w\frac{\partial w}{\partial z}\right)=-\frac{\partial \rho}{\partial z}+u\left(\frac{\partial \tau_{xz}}{\partial x}+\frac{\partial \tau_{yz}}{\partial y}+\frac{\partial \tau_{zz}}{\partial z}\right)+\rho F_z \quad (12)$$

In the above equations, μ represents the kinetic viscosity; τ_{xx}, τ_{yy} and τ_{zz} are the components of viscous force; F_x, F_y and F_z are the components of the volumetric force respectively [16].

2.2.2.3 Numerical Equations

Generally, the laminar fluid flows are less intricate compared to turbulent fluid flows; as a result, they can be solved using the Navier-Stokes equations. In contrast, turbulent fluid flows are encountered more often in engineering applications and are dominated by 3-dimensional, highly unsteady structures generated by blade curvature [16]. The analytical calculations using Navier-Stokes equations are good for solution approximations; however, the major demerit is that they do not explicitly detail the complexities associated with the turbulent fluid flows, as the centrifugal pump will be operating.

For laminar flow, the N-S equations are sufficient for resolution. However, in practical engineering scenarios, fluid flow is predominantly turbulent, which represents a complex flow phenomenon commonly encountered in such applications. The N-S equations do not fully capture the intricacies of turbulent fluid flow during computational analysis [16]. In turbulent flow conditions, it is acceptable to disregard the details of fluctuations and instead perform suitable averaging of the N-S equations. The resulting averaged flow equations, along with the accompanying mathematical formulas, form the basis of a turbulent model.

To predict the performance of the centrifugal pump accurately, it is imperative to develop a precise and highly dependent CFD model for numerical simulation. Globally, academia and engineering-focused industrial corporations utilize the "two-equation turbulence models (standard k-ε model, RNG k-ε model, realizable k-ε model) as they allow the determination of both a turbulent length and time scale by solving two separate transport equations" [15]. Another crucial model extensively used for numerical simulations is the shear stress transport (SST) k-ω model. The merit of using the SST k-ω model is that it integrates the standard k-ε model features pertaining to the computations of far fields with the robustness of the SST k-ω model's near-wall region computations [15]. This

integration is regarded as highly precise, as the numerically computed results closely match the experimental results [16].

Below are the SST k-ω model equations which have a similitude form to the standard k-ω model.

$$\frac{\partial}{\partial t}(\rho k) + \frac{\partial}{\partial x_i}(\rho k u_i) = \frac{\partial}{\partial x_j}\left[\Gamma_k \frac{\partial k}{\partial x_j}\right] + \bar{G}_k - Y_m + S_k \quad (13)$$

$$\frac{\partial}{\partial t}(\rho \omega) + \frac{\partial}{\partial x_j}(\rho \omega u_j) = \frac{\partial}{\partial x_j}\left[\Gamma_\omega \frac{\partial \omega}{\partial x_j}\right] + G_\omega - Y_\omega + D_\omega + S_\omega \quad (14)$$

In equation (13), the turbulence kinetic energy is represented by $\bar{G}_k$. G_ω represents the generation of ω. Γ_k and Γ_ω represent the effective diffusivity of k and ω, respectively. Y_k and Y_ω represent the dissipation of k and ω due to turbulence. D_ω represents the cross-diffusion term, S_k and S_ω are user-defined source terms [17].

2.3 BOUNDARY CONDITIONS

The fine meshing of the pump and impeller was generated using ANSYS CFD tool. To set up the simulation of the centrifugal pump the steady state analysis was applied. The impeller was defined as a rotating frame of reference with a rotational speed of 1450 rpm and the volute was defined as a stationary component. The $\kappa\omega$ turbulence (shear stress transport model) was used for the pump evaluation; this method has been proved to replicate realistic scenarios [18]. The inlet and outlet boundary conditions were defined as follows: 0 absolute pressure at the pump inlet and the variable mass flow rate of 77.8 to 170 kg/s at the volute exit. The frozen rotor interface was used in the analysis.

The boundary condition of no-slip wall was applied on the impeller shroud, hub and vanes. The solver control settings were as follows: convergence iterations of a maximum of 1000, physical timescale of $10e^{-2}$ and precision residuals of $1e^{-5}$ were applied.

3.0 FINDINGS AND DISCUSSION

3.1 Tabulated Results for 4 to 10 Blade Impellers

The centrifugal pump was simulated through the CFD tool utilising varying mass flow rates and number of blades, the rest of parameters were constant throughout the analysis. Table 2 to 5 depicts the output results extracted from post processing module of ANSYS software.

It is possible to plot the performance curves of the centrifugal pump with the data from Table 2 to 5 and conduct a comparison to determine the optimal design point (best efficiency point) utilising the head rise, efficiency, power of the specific impeller configuration.

ISSN 2180-1053 e-ISSN 2289-8123 Vol.17 No.2

Table 2. Results for 4-Blades Impeller

Four Blades Impeller			
Flow Rate m^3/hr	Head (m)	Efficiency (η%)	Power (KW)
280	21.591	89.388	11.904
324	19.928	90.662	12.941
396	18.086	92.455	14.181
468	15.177	92.23	14.647
540	12.954	91.441	14.418
612	10.912	89.806	13.378

Table 3. Results for 6-Blades Impelle

Six Blades Impeller			
Flow Rate m^3/hr	Head (m)	Efficiency (η%)	Power (KW)
280	21.88	88.16	14.302
324	20.826	89.69	15.652
396	19.931	93.274	17.731
468	17.36	92.349	18.616
540	14.803	90.415	18.745
612	12.217	87.222	17.981

Table 4. Results for 8-Blades Impeller

Eight Blades Impeller			
Flow Rate m^3/hr	Head (m)	Efficiency (η%)	Power (KW)
280	21.469	85.892	18.944
324	21.13	89.36	20.491
396	20.208	92.21	23.052
468	17.69	90.879	23.968
540	14.98	87.798	24.083
612	11.819	82.189	23.352

Table 5. Results for 10-Blades Impeller

Ten Blades Impeller			
Flow Rate m^3/hr	Head (m)	Efficiency (η%)	Power (KW)
280	23.283	89.54	27.644
324	22.038	90.186	29.099
396	19.682	89.83	31.648
468	16.615	86.78	31.465
540	13.316	81.51	31.261
612	9.589	71.7	30.383

The head and volumetric flow rate graph shows a combined illustration of the centrifugal pump's hydraulic performance fundamentals, depicting how the energy added by the impeller the rotating part that moves the fluid affects the liquid. It also shows how friction losses increase as the volumetric flow rate the amount of fluid passing through per unit time rises, explicitly representing departures from the ideal Euler head the theoretical maximum height to which the pump can raise the fluid. The graph's shape reflects the centrifugal pump's stability characteristics, helping to identify regions that allow stable operation and areas susceptible to problems like rotation stall when parts of the flow stop moving properly, surge sudden changes in flow, and fluid recirculation instabilities.

There are several types of industrial pumps, and all must operate at the point where the head and flow rate curve meet the hydraulic resistance system's curve representing the resistance created by the system's pipes and components. This intersection point predicts how changes in valve positions, pipe design, and network setups shift the operating condition. If industrial pumps include monitoring devices for efficiency and power, the BEP Best Efficiency Point, where the pump is most efficient can be precisely identified on the head and flow rate curve. This helps spot how running the pump outside its optimal range can increase the risk of issues such as cavitation formation of vapor bubbles, vibrations, mechanical stress, and pump damage. Additionally, the head and volumetric flow rate relationship underpins similarity laws in turbomachinery rules relating models to actual devices, enabling predictions from scale models to full-size pump performance. Figures 1 to 3 depict performance curves of centrifugal pump operated with 4, 6, 8 and 10-blade impeller. Furthermore, detailing the merits and demerits of these configurations.

ISSN 2180-1053 e-ISSN 2289-8123 Vol.17 No.2

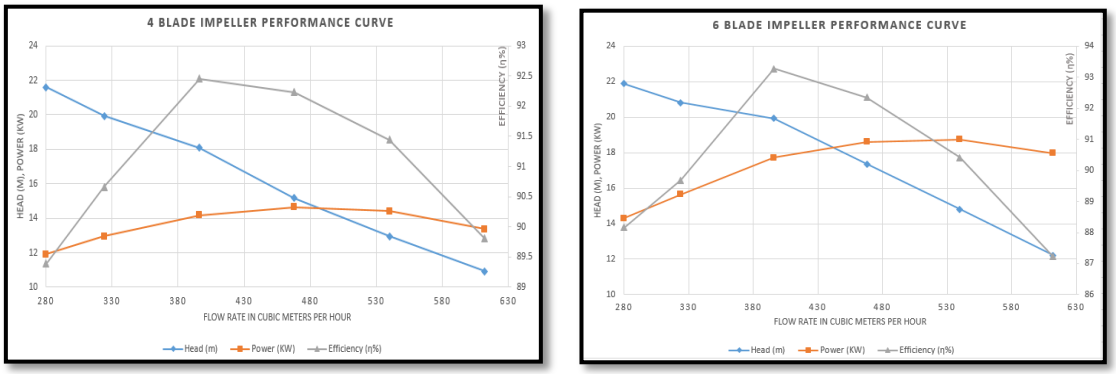

(a) (b)

Figure 1 (a) Head, Power, Efficiency vs Volumetric Flow Rate Curve for the 4-Blade Impeller. (b) Head, Power, Efficiency vs Volumetric Flow Rate Curve for the 6-Blade Impeller.

It can be observed from figure 1a that to produce a head of 21.591 m, the system efficiency of 89,388 % is generated. The gradual increments in volumetric flow rate result in an increase in efficiency of the pump until the flow rate of 396 m^3/hr where the system head is recorded to be 19.931 m at the maximum efficiency of 92.455 %, beyond this point the efficiency of the system continues to drop gradually. The power curve increase until the flow rate of 468 m^3/hr, then gradually decline as the efficiency drops.

In figure 1b, it is observed that the head of 21.88 m is produced when the system efficiency of 88,16 % is generated. The gradual increments in flow rate result in an increase in efficiency of the pump until the flow rate of 396 m^3/hr where the system head is recorded to be 19.931 m at the maximum efficiency of 93.274 %, beyond this design point the efficiency of the system continues to drop gradually. The power curve increase until the flow rate of 540 m^3/hr, then continues to drop.

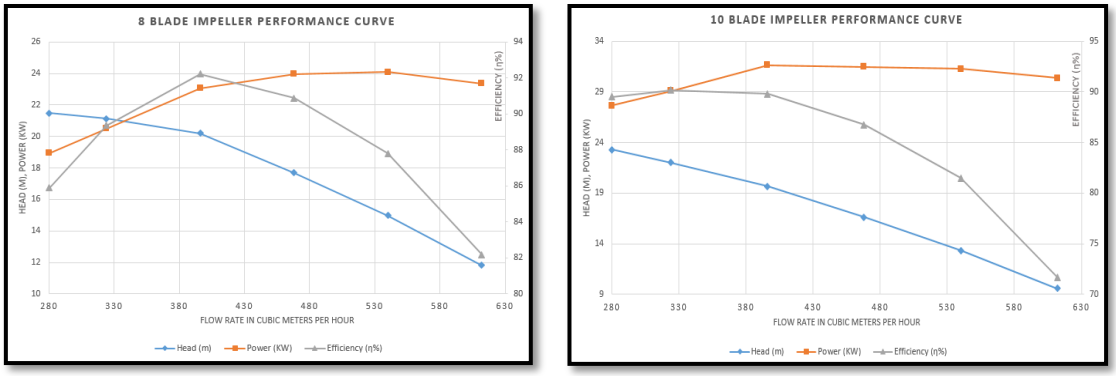

(a) (b)

Figure 2 (a) Head, Power, Efficiency vs Volumetric Flow Rate Curve for the 8 Blade Impeller. Figure 2 (b) Head, Power, Efficiency vs Volumetric Flow Rate Curve for the 10 Blade Impeller.

In Figure 2(a), it is seen that the head of 21.469 m is produced when the system efficiency of 85.892 % is generated. The gradual increments in flow rate result in an increase in efficiency of the pump until the flow rate of 396 m^3/hr where the system head is recorded to be 22.038 m at the maximum efficiency of 92.21 %, beyond this design point the efficiency of the system continues to drop gradually. The power curve increase until the

ISSN 2180-1053 e-ISSN 2289-8123 Vol.17 No.2

flow rate of 540 m³/hr, then continues to drop showing similar characteristics to the 6-blade impeller system.

In Figure 2(b), it can be noticed that the head of 23.283 m is produced when the system efficiency of 89.54 % is generated. The gradual increments in flow rate result in an increase in efficiency of the pump until the flow rate of 324 m³/hr where the system head is recorded to be 20.208 m at the maximum efficiency of 90.186 %, beyond this design point the efficiency of the system continues to drop steeply in comparison to 4, 6 and 8-blade impeller configurations. The power curve increase until the flow rate of 396 m³/hr, then continues to drop.

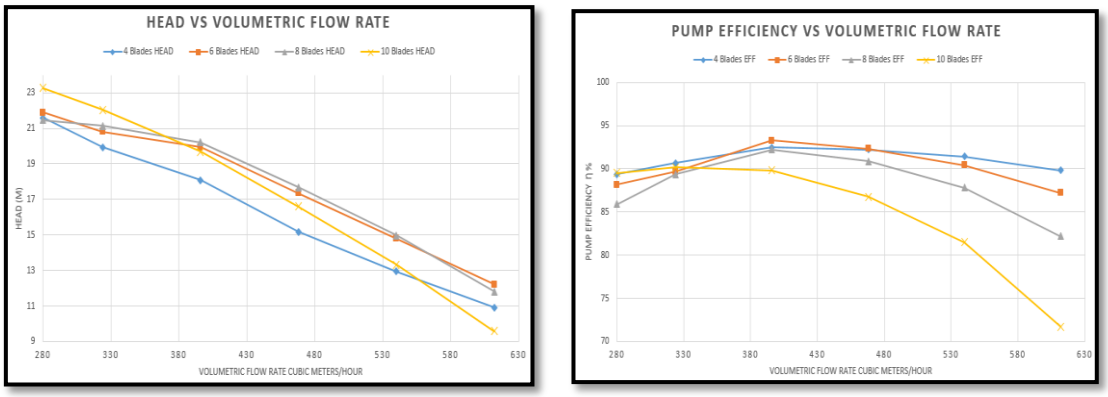

(a) (b)

Figure 3(a) Head vs Volumetric Flow Rate Curve. Figure 3(b). Efficiency vs Volumetric Flow Rate Curve.

In Figure 3(a) it can be observed from the initial flow rate of 280 m³/hr, the impeller with 10 blades has the highest head slightly north of 23 m, followed by 6-blade impeller while the lowest head value is recorded for impeller with 8 blades. When the flow rate is gradually increased towards 612 m³/hr it further observed that the 10-blade impeller's head takes a steep decline in comparison to the 6 and 8-blade impellers which display a gradual decrease. The 4 blade impeller head remains low for 4 gradual consecutive increments in flow rates in comparison with other impellers.

It can be further observed from Figure 3(b) that the 6-blade impeller has the best efficiency at design point followed by 4 and 8 blade impellers while the 10-blade impeller has the lowest efficiency. The increment in flow rate results in the 4-blade impeller showing stable performance followed by the 6-blade while the 8 and 10-blade impellers show steep decline in efficiency curve.

3.2 Pressure Profiles for 4 to 10-Blade Impellers

The pressure distribution for the 4 to 10 blade impellers increases gradually from the inlet to the stream wise path within the impeller channel and lastly the outlet. It can further be noted that the higher-pressure vicinity is observed on the pressure side in comparison to the suction side on the impeller blades [19].

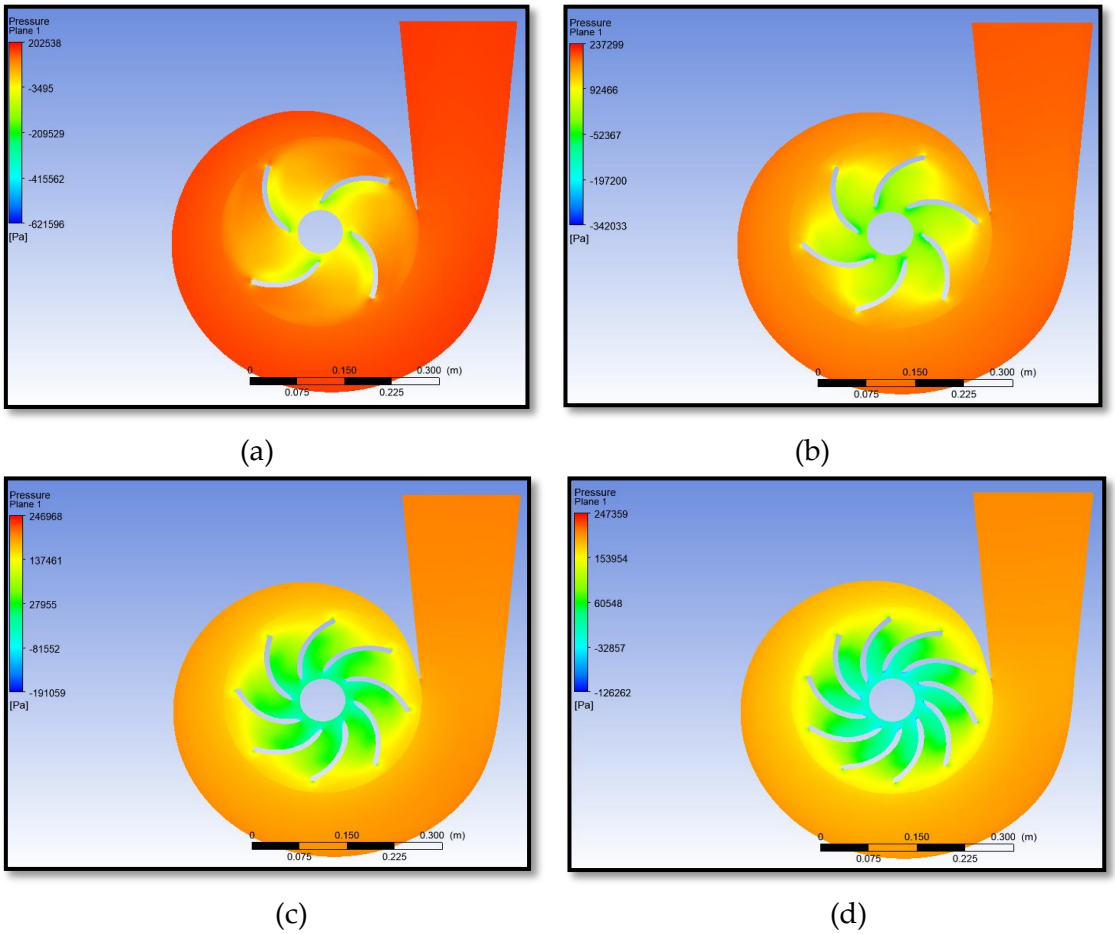

Figure 4(a). Four Blade Impeller Pressure. (b) Six Blade Impeller Pressure. (c). Eight Blade Impeller Pressure. (d). Ten Blade Impeller Pressure.

The static pressure for all pump impellers at the volute exits points is higher when the volumetric flow rate is minimum, in contrast the static pressure exhibits a minimal value when the volumetric flow rate is higher. Furthermore, from Figure 4(a) to (d) it can be seen that when the number of blades is increased, there is also an increase in static pressure at the volute exit point explicitly indicating that the number of blades have effect on the performance characteristics of the pump.

It can be observed that there is distinctiveness in the pressure contours of a 4-blade impeller configuration, as depicted in Figure 4(a), compared to those of the 6, 8, and 10-blade impeller configurations. This uniqueness in pressure contours stems from the wide impeller blade passages, which reduce blade interference and lead to quasi-uniform radial flow diffusion. High head in centrifugal pumps cannot be substantially achieved with fewer impeller blades; they also result in an increase in slip relative to the Euler prediction. Furthermore, they stimulate a stable pressure distribution owing to the weak, localised blade-induced pressure perturbations. Consequently, the pressure contour variations for the 4-blade impeller are less noticeable, as global centrifugal acceleration substantially governs the pressure field relative to individual blade loading.

3.3 Velocity Profiles for 4 to 10 Blade Impellers

Figure 5(a) depict a velocity profile for an impeller with 4 blades, as it can be observed the categorization of energy inside the channel results from a wider pitch ratio which

ISSN 2180-1053 e-ISSN 2289-8123 Vol.17 No.2

eventually leads to Jet/Wake at the impeller channel exit. The non-uniformity of the fluid flow at the exit of the channel stems from the increment of secondary losses, generally increasing the overall losses irrespective of lowering the frictional losses caused by the number of blades [8].

The 4-blade impeller has a large pitch ratio, the fundamental fluid mechanics mechanisms governing rotating internal flows make a jet/wake structure at the channel exit almost unavoidable. The wide pitch reduces the confinement of the flow, thereby weakening inter-blade pressure coupling and allowing strong cross-passage pressure gradients to persist. Under rotation, the fluid must simultaneously satisfy radial equilibrium and circumferential momentum conservation; this induces curvature driven centrifugal forces and Coriolis accelerations that distort the velocity field within each passage. Fluid near the suction side experiences favorable pressure gradients and streamline curvature that enhance convective acceleration, producing a high momentum jet.

In contrast, fluid near the pressure side encounters adverse pressure gradients that intensify boundary layer growth, promote secondary vorticity, and reduce local kinetic energy, forming a momentum deficient wake. Because viscous diffusion operates on much longer timescales than the convective and inertial processes governing the rotating frame, momentum cannot homogenize across the widely spaced blades before the flow exits. The resulting exit profile characterized by coexisting high energy jets and low energy wakes is therefore a direct manifestation of classical rotating flow physics: imbalance between pressure gradient forces, curvature induced inertial effects, and the limited capacity of viscous transport to smooth momentum within a rotating, spatially nonuniform channel.

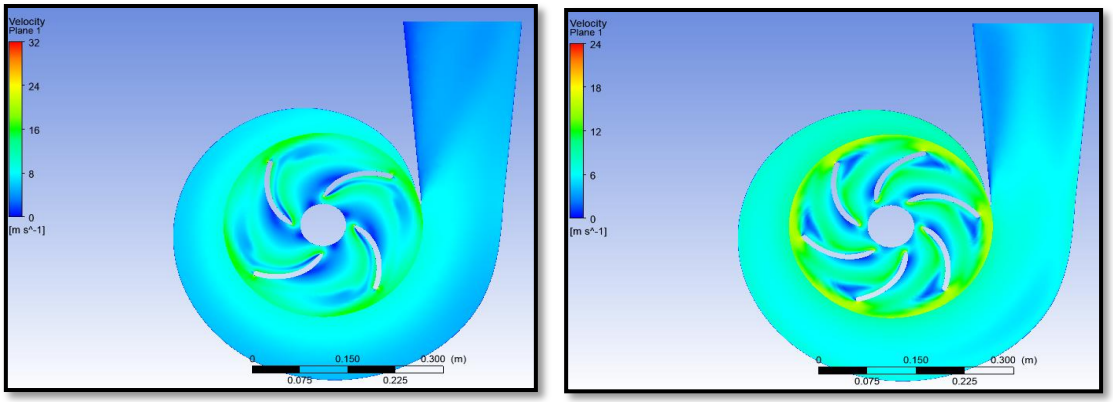

(a) (b)

ISSN 2180-1053 e-ISSN 2289-8123 Vol.17 No.2

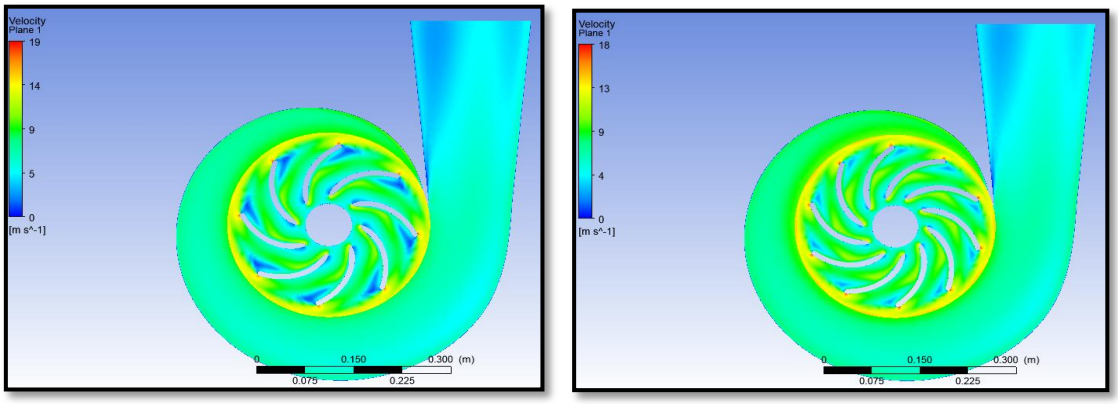

(c) (d)

Figure 5(a). Four Blade Impeller Velocity Profile. (b). Six Blade Impeller Velocity Profile. (c). Eight Blade Impeller Velocity Profile. (d). Ten Blade Impeller Velocity Profile.

The impeller with 6 blades as depicted in Figure 5(b) shows the marginal increment with respect to the blades friction loss. The marginal closing of pitch ratio resulted in a uniform fluid flow at the channel exit which further translated to a decline in energy categorization and the development of Jet/Wake distribution. The velocity at the channel exit is uniform in comparison to the 4-blade impeller configuration.

Figure 5(c) and (d) display similar characteristics pertaining to the fluid flow at the channel exit. It can be explicitly observed that there is formation of mixing losses at the impeller exit channel for figure 5(c) denoted by the yellowish profile, with respect to Figure 5(d) there is a gradual change in the yellowish profile to red indicating high mixing losses in comparison to all other blade configurations. The 10-blade impeller exhibit higher frictional losses due to high velocity profiles closer to the blades exit. Moreover, these losses can be clearly observed from the efficiency curves plotted in Figure 3b.

In Table 6, the power consumption of the 4-blade impeller is the lowest followed by the 6, then 8 while the 10-blade impeller displays highest consumption in comparison to other blade configurations. At the Best Efficiency Point (BEP), centrifugal pumps function under conditions that minimize hydraulic losses and maximize the conversion of mechanical input into fluid kinetic and pressure energy. In fluid mechanics, the BEP represents optimal flow incidence at the impeller inlet and a uniform exit velocity distribution, which reduces flow separation, recirculation, and secondary flows within the impeller passages. The number of blades, specifically 4, 6, 8, or 10, significantly affects pressure rise, velocity distribution, and energy dissipation. Impellers with fewer blades, such as four, typically exhibit greater velocity slip and uneven pressure distribution along the impeller periphery. This can induce localized turbulence and secondary flows near the shroud, thereby reducing BEP efficiency. Increasing the blade count to six or eight generally improves the uniformity of the relative velocity triangles, reduces flow separation, and enhances energy transfer to the fluid. However, excessive blade numbers can increase blockage and frictional losses, offsetting these gains. The 10-blade configuration usually provide the smoothest pressure gradients and minimal recirculation, but at the expense of higher skin friction and increased hydraulic losses within the blade passages.

ISSN 2180-1053 e-ISSN 2289-8123 Vol.17 No.2

From a fluid mechanics perspective, the BEP for each blade configuration can be evaluated using velocity triangle relationships, radial and tangential velocity components, and the resulting head generation. At BEP, the relative flow closely aligns with the blade angle, which reduces incidence losses and limits secondary vortices near the leading edge. In the case of a 4-blade impeller, significant velocity lip and higher peripheral velocity gradients are observed, resulting in larger wake regions and non-uniform flow at the exit. The 6- and 8-blade impellers mitigate these non-uniformities, enabling more uniform radial momentum transfer and smoother interaction with the volute, thereby enhancing hydraulic efficiency. A 10-blade impeller further homogenizes exit flow and minimizes secondary flows, but also increases blockage effects and wall shear stress, which slightly raises frictional head losses. As a result, the BEP shifts subtly with blade count, reflecting a trade-off between minimizing incidence induced turbulence and mitigating viscous and blockage losses. This dynamic demonstrates the complex interplay among impeller geometry, fluid momentum, and energy conversion efficiency in centrifugal pump design.

Table 6. Results of Pumps at Best Efficiency Points

Rotational Speed (RPM)	Number of Blades	Flow Rate (m^3/hr)	Head (m)	Efficiency (%)	Power (KW)
1450	4	396	18.086	92.455	14.181
1450	6	396	19.931	93.274	17.731
1450	8	396	20.208	92.210	23.052
1450	10	324	22.038	90.186	29.099

City of Tshwane tariff for bulk supply of electricity according to NERSA is 161Cent/KWH [20]. The conversion of Cents to South African Rand is as follows:
Rand = (161 Cent/100Cent KWH) = R1.61/KWH

The operational cost of a centrifugal pump is significantly influenced by the number of impeller blades due to the interaction between viscous dissipation and hydraulic head generation as indicated in Table 7. The input powers at BEP are 14.184kW for 4 blades, 17.731kW for 6 blades, 23.052kW for 8 blades, and 29.099kW for 10 blades. The corresponding daily operating costs for 8 hours of operation at ZAR 1.61/kWh are ZAR 182.8, ZAR 228.3, ZAR 296.8, and ZAR 374.7, respectively. These values translate to monthly costs of ZAR 5662, ZAR 6851, ZAR 8907, and ZAR 14618.

Table 7. Cost of operating pump at Best Efficiency Points

Number of Blades	Power (KW)	Rand/KWH	Hours	Rand/Month
4	14.181	1.61	8	5662
6	17.731	1.61	8	6851
8	23.052	1.61	8	8907
10	29.099	1.61	8	14618

According to fluid mechanics principles, increasing the number of blades in a centrifugal pump enhances the slip factor, thereby improving the developed head and providing more effective flow guidance. However, this increase reduces overall hydraulic efficiency per unit shaft power due to narrower blade passages, enlarged boundary layer interactions, increased wall shearing, and greater viscous losses. A 4-blade impeller results in minimal viscous losses and wider passages but experiences less effective flow

guidance, increased secondary flows, and lower head. Consequently, it achieves only moderate efficiency at BEP despite lower power consumption.

In distinctiveness, the number of blades ranging from 8 to 10 is able to accomplish high head with well-aligned fluid flow, low secondary vortices, but suffers substantial power consumption owing to the blockage and friction losses, which translates to higher costs of centrifugal pump operation. The pump impeller with 6 blades strikes an optimal compromise at BEP, explicitly balancing enough slip factor to achieve high head with reasonable viscous dissipation. This maximizes hydraulic output per unit energy cost and demonstrates the critical role of blade geometry in the energetic and economic performance of centrifugal pumps.

4.0 CONCLUSION

The ANSYS CFD software was utilised to examine how the various number of blades have significant effect on the centrifugal pump performance specifically monitoring the head, efficiency, power consumption and pressure. The following parameters were constant: inlet and exit blade angles, rotational speed, diameter of impeller, thickness of blades and inlet diameter. The iteration of parameters applied was the number of blades and the volumetric flow rate.

i. The pressure distribution for all blade's configuration increase from the inlet and reach a higher value at the volute exit as dynamic energy is converted to pressure energy.
ii. The pressure is higher when the volumetric flow rate is minimum and gradually drops with increasing volumetric flow rate.
iii. An increase in number of blades translates to an increase in head and pressure of the system. Furthermore, it was discovered that when the number of blades are increased, the power consumption of the pump also increases.
iv. The hydraulic efficiency and volumetric flow rate are substantially influenced by the number of blades of the impeller for the centrifugal pump at BEP. The optimal head is limited by the unconstrained fluid flows resulting largely from wide passages as a consequence of a 4-blade impeller, severe secondary flows, and unstable velocity distributions. The hydraulic efficiency and uniform volumetric flow rate are maximized by the 6-blade impeller due to the optimized relative velocities, which are aligned with the blade angles, thereby reducing slip factor and recirculation in the pump. The high head is achieved by the blade configuration from 8 to 10 since they are capable of yielding well-guided fluid flows with lower secondary losses, but then develop substantial viscous shear and passage blockages, which results in some extent restricted volumetric flow. Therefore, a 6-blade configuration represents the optimal balance between volumetric flow, flow uniformity, and efficiency, making it the preferred design choice for centrifugal pumps

ACKNOWLEDMENTS

The authors would like to extend their gratitude to Tshwane University of Technology for providing the facility to complete this research activity. The design and finite element analysis of the centrifugal pump were conducted utilizing the CFD module of ANSYS software.

REFERENCES

[1] E. P. Deepak, S. Sankar, T. Thomas and K. V. Sreejith, "Analysis of a Centrifugal Pump Impeller using ANSYS," *International Journal of Innovative Research, Science, Engineering and Technology*, vol. 7, no. 5, p. 7, 2018.

[2] H. M. P. Rosa and B. S. Emerick, "CFD Simulation on Centrifugal Pump Impeller with Splitter Blades," *Brazilian Journal of Agricultural and Environmental Engineering*, p. 5, 2019.

[3] R. Lopez, M. Vaca, H. Terres, A. Lizardi, S. Chaves and M. Garcia, "Performance simulation of a radial flow type impeller of centrifugal pumps using CFD", *Journal of Physics: Conference Series*, vol. 792, no. 1, p. 012029, 2017.

[4] M. S. Rajmane and S. P. Kallurkar, "Study of Stresses Developed on the Impeller of Centrifugal Pump at Different Speed using Ansys", *International Journal of Engineering Research & Technology,* vol. 5, no. 01, 2017.

[5] S. R. Muttalli, S. Agrawal and H. Warudkar, "CFD Simulation of Centrifugal Pump Impeller Using ANSYS-CFX," *International Journal of Innovative Research in Science Engineering and Technology*, vol. 3, no. 8, p. 9, 2014.

[6] S. Marathe and R. Saxena, "Numerical Analysis of Effect of Exit Blade Angle on Cavitation in Centrifugal Pump," *International Journal of Mechanical Engineering and Technology*, vol. 3, no. 4, p. 8, 2013.

[7] K. S. Hayder, "Numerical Analysis of the Effect of Blades on the Centrifugal Pump Performance at Constant Parameters," *International Journal of Mechanical Engineering and Technology*, vol. 6, no. 8, p. 13, 2015.

[8] G. R. Eliyamin, M. A. Bassily, K. Y. Khalil and M. S. Gomaa, "Effect of Impeller Blades Number on the Performance of a Centrifugal Pump," *Alexandria Engineering Journal,* p. 11, 2019.

[9] E. E. Enemugha, S. B. Mohd and B. G. Nik Nazri, "The Effects of Impeller Blade Count on Centrifugal Pump Performance and Efficiency Under Different Operating Conditions: A Comparison of Numerical Prediction," *International Journal for Research in Applied Science & Engineering Technology*, vol. 13, no. 4, p. 14, 2025.

[10] D. Venkatratnam, "Performance Analysis of Centrifugal Pump by Using CFD," *International Journal of Mechanical Engineering and Technology*, vol. 8, no. 10, p. 10, 2017.

[11] N. DInesh, C. J. Nakul, R. Vishnu, A. Haleem and M. Vishnu, "Design and CFD Analysis of Centrifugal Pump," *International Journal of Engineering Research & Technology*, vol. 9, no. 10, p. 5, 2021.

[12] E. Dick, J. Vierendeels, S. Serbruyns and J. Vande Voorde, "Performance Prediction of Centrifugal Pumps with CFD-Tools," Sint-Pietersnieuwstraat, 2001.

[13] P. Raut, R. Rathod, R. Tidke, N. Rathod, S. Rokade and N. Kulkarni, "Design and CFD Analysis of Centrifugal Pump," *International Journal for Research in Applied Science & Engineering Technology*, vol. 10, no. 12, p. 11, 2022.

[14] C. F. Meyer, Applications of Fluid Mechanics Part 2, Pretoria: CM TEK Lecture Materials cc, 2015.

[15] P. M. Modi and S. M. Seth, Hydraulics and Fluids Mechanics including Hydraulic Machines, Delhi, 2017.

[16] Y. Long, H. Wang, R. Wang, B. He and Q. Fu, "Effect of Induced Wheel and Impeller Inlet Diameter on the Hydrodynamic Performance of High-speed Centrifugal Pumps," *Journal of Applied Fluid Mechanics*, vol. 17, no. 11, p. 24, 2024.

[17] ANSYS, "ANSYShelp," 01 11 2011. [Online]. Available: https://ansyshelp.ansys.com/public/account/secured?returnurl=/Views/Secured/corp/ v242 /en/flu_th/flu_th.html. [Accessed 01 12 2025].

[18] L. Zhou, W. Shi and S. Wu, "Performance Optimization in a Centrifugal Pump Impeller by Orthogonal Experiment and Numerical Simulation," *Advances in Mechanical Engineering*, p. 7, 2013.

[19] T. A. Meakhail, M. Salem and I. Shafie, "Steady and unsteady flow inside a centrifugal pump for two different impellers," *International Journal of Energy and Power Engineering*, p. 13, 2014.

[20] NERSA, "NERSA," 2024. [Online]. Available: https://www.nersa.org.za/wp-content/uploads/bsk-pdf-manager/2022/10/Approved-Municipal-Electricity-Tariffs-2022- 23.pdf. [Accessed 20 06 2024].